Exploring parameter constraints on quintessential dark energy: The pseudo-Nambu-Goldstone-boson model

Augusta Abrahamse, Andreas Albrecht, Michael Barnard, and Brandon Bozek
Physics Department, University of California, Davis, California, USA
(Received 17 January 2008; published 5 May 2008)

We analyze the constraining power of future dark energy experiments for pseudo-Nambu-Goldstone-boson (PNGB) quintessence. Following the Dark Energy Task Force (DETF) methodology, we forecast data for three experimental stages: Stage 2 represents in-progress projects relevant to dark energy; Stage 3 refers to medium-sized experiments; Stage 4 comprises larger projects. We determine the posterior probability distribution for the parameters of the PNGB model using Markov Chain Monte Carlo analysis. Utilizing data generated on a ΛCDM cosmology, we find that the relative power of the different data stages on PNGB quintessence is roughly comparable to the DETF results for the $w_0 - w_a$ parametrization of dark energy. We also generate data based on a PNGB cosmological model that is consistent with a ΛCDM fiducial model at Stage 2. We find that Stage 4 data based on this PNGB fiducial model will rule out a cosmological constant by at least 3σ.

DOI: 10.1103/PhysRevD.77.103503 PACS numbers: 95.36.+x, 98.80.Es

I. INTRODUCTION

A growing number of observations indicate that the expansion of the universe is accelerating. Given our current understanding of physics, this phenomenon is a mystery. If Einstein's gravity is correct, then it appears that approximately 70% of the energy density of the universe is in the form of a "dark energy." Although there are many ideas of what the dark energy could be, as of yet, none of them stands out as being particularly compelling. Future observations will be crucial to developing a theoretical understanding of dark energy.

A number of new observational efforts have been proposed to probe the nature of dark energy, but evaluating the impact of a given proposal is complicated by our poor theoretical understanding of dark energy. In light of this issue, a number of model independent methods have been used to explore these issues (see, for example, [1,2]). Notably, the Dark Energy Task Force (DETF) produced a report in which they used the $w_o - w_a$ parametrization of the equation of state evolution in terms of the scale factor, $w(a) = w_o + w_a(1 - a)$ [3]. The constraints on the parameters w_o and w_a were interpreted in terms of a "figure of merit" (FoM) designed to quantify the power of future data and guide the selection and planning of different observational programs. Improvements in the DETF FoM between experiments indicate increased sensitivity to possible dynamical evolution of the dark energy. This is crucial information, since current data is consistent with a cosmological constant and any detection of a deviation from a cosmological constant would have a tremendous impact. There are, however, a number of questions left unanswered when the dark energy is modeled using abstract parameters such as $w_0 - w_a$ that are perhaps better addressed with the analysis of actual theoretical models of dark energy.

First of all, the $w_o - w_a$ parametrization is simplistic and not based on a physically motivated model of dark energy. Although simplicity is part of the appeal of this parametrization, some of the most popular dark energy models exhibit behavior that cannot be described by the $w_o - w_a$ parametrization. The pseudo-Nambu-Goldstone-boson (PNGB) quintessence model considered in this paper, for instance, allows equations of state that cannot be approximated by the $w_o - w_a$ parametrization, as shown in Fig. 1.

Conversely, the $w_o - w_a$ parametrization may allow solutions that do not correspond to a physically motivated model of dark energy. Because of these issues, one could wonder whether the DETF FoM's are somehow misleading. Various concerns with the DETF analysis have already been explored. Albrecht and Bernstein used a more complex parametrization of the scale factor to check the validity of the $w_0 - w_a$ approximation [4], and Huterer and Peiris considered a generalized class of scalar field models [5]. Additionally, it has been suggested that the DETF data models might be improved (see, for instance, [6]).

As of yet, however, no actual proposed models of dynamical dark energy have been considered in terms of future data. Given the issues above, such an analysis is an important compliment to existing work. Of course all specific models of dark energy are suspect for various reasons, and one can just as well argue that it is better to make the case for new experiments in a more abstract parameter space rather than tying our future efforts to specific models that themselves are problematic. Rather than "take a side" in this discussion, our position is that given the diversity of views on the subject, a model-based assessment will have an important role in an overall assessment of an observational program.

In this paper we consider the pseudo-Nambu-Goldstone-boson quintessence model of dark energy [7]. As one of the

 © 2008 The American Physical Society

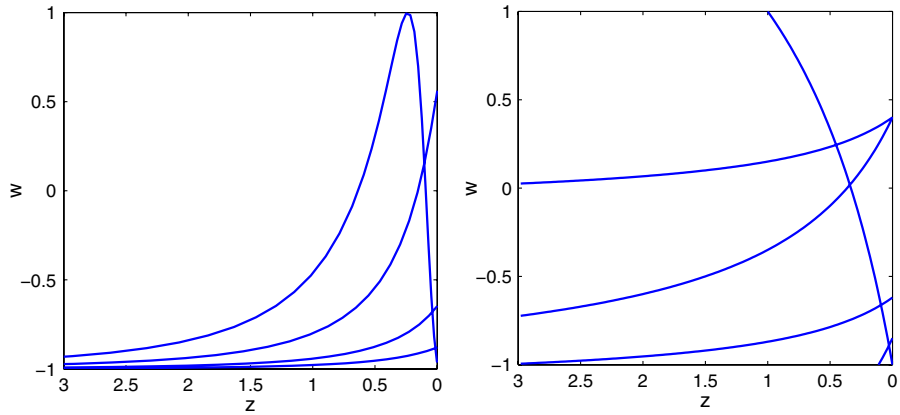

FIG. 1 (color online). Examples of possible equations of state for PNGB quintessence (left panel). Attempts to imitate this behavior with $w(z)$ curves for the $w_0 - w_a$ parametrization are depicted on the right.

most well-motivated quintessence models from a particle physics perspective, it is a worthwhile one to study. We use the data models forecasted by the DETF and generate two types of data sets, one based on a ΛCDM background cosmology and one based on a background cosmology with PNGB dark energy using a specific fiducial set of PNGB parameters. We determine the probability space for the PNGB parameters given the data using Markov Chain Monte Carlo analysis. This paper is part of a series of papers in which a number of quintessence models are analyzed in this manner [8,9].

We show that the allowed regions of parameter space shrink as we progress from Stage 2 to Stage 3 to Stage 4 data in much the same manner as was seen by the DETF in the $w_0 - w_a$ space. This result holds for both ΛCDM and the PNGB data models. Additionally, with our choice of PNGB fiducial background model, we demonstrate the ability of Stage 4 data to discriminate between a universe described by a cosmological constant and one containing an evolving PNGB field. As cosmological data continues to improve, careful analysis of specific dark energy models using real data will become more and more relevant. MCMC analysis can be computationally intensive and time consuming. Since future work in this area is likely to encounter similar challenges, we discuss some of the difficulties we discovered and solutions we implemented in our MCMC exploration of PNGB parameter space.

II. PNGB QUINTESSENCE

Quintessence models of dark energy are popular contenders for explaining the current acceleration of the universe [10–12]. Although the cosmological constant is regarded by many to be the simplest theory of the dark energy, the required value of the cosmological constant appears to be many orders of magnitude too small in naive particle theory estimates. In quintessence models this problem is not solved. Instead it is generally sidestepped by assuming some unknown mechanism sets the vacuum energy to exactly zero, and the dark energy is due to a scalar field evolving in a pressure dominated state. As such fields can appear in many proposed "fundamental theories," and as the mechanism mimics ideas familiar from cosmic inflation, quintessence models are regarded by many (but certainly not by everyone [13]) to be at least as plausible as a cosmological constant [14,15].

Here the quintessence field is presumed to be homogeneous in space, and is described by some scalar degree of freedom ϕ and a potential $V(\phi)$ which governs the field's evolution. In a Friedmann-Robertson-Walker (FRW) spacetime, the field's evolution is given by

$$\ddot{\phi} + 3H\dot{\phi} + \frac{dV}{d\phi} = 0, \tag{1}$$

where

$$H = \frac{\dot{a}}{a} \tag{2}$$

and

$$H^2 = \frac{1}{3M_p^2}(\rho_r + \rho_m + \rho_\phi + \rho_k), \tag{3}$$

where M_P is the reduced Planck mass, ρ_r is the energy density of radiation, ρ_m is the energy density of nonrelativistic matter, and ρ_k is the effective energy density of spacetime curvature. The energy density and pressure associated with the field are

$$\rho_\phi = \tfrac{1}{2}\dot{\phi}^2 + V(\phi), \qquad P_\phi = \tfrac{1}{2}\dot{\phi}^2 - V(\phi) \tag{4}$$

and the equation of state w is given by

$$w \equiv \frac{P_\phi}{\rho_\phi}. \tag{5}$$

If the potential energy dominates the energy of the field, then as can be seen in Eq. (4) the pressure will be negative and in some cases can be sufficiently so to give rise to acceleration as the universe expands.

The PNGB model of quintessence is considered compelling because it is one of the few models that seems natural from the perspective of $4-D$ effective field theory. In order to fit current observations, the quintessence field must behave at late times approximately as a cosmological constant. It must be rolling on its potential without too much contribution from kinetic energy, and the value of the potential must be close to the observed value of the dark energy density, which is on the order of the critical density of the universe $\rho_c = 3H_0^2 m_p^2 = 1.88 \times 10^{-26} h^2\,\mathrm{kg/m^3}$ or $2.3 \times 10^{-120} h^2$ in reduced Planck units, where $h = H_0/100$. These considerations require the field to be nearly massless and the potential to be extraordinarily flat from the point of view of particle physics. In general, radiative corrections generate large mass renormalizations at each order of perturbation theory unless symmetries exist to suppress this effect [16–18]. In order for such fields to seem reasonable, at least on a technical level, their small masses must be protected by symmetries such that when the masses are set to zero they cannot be generated in any order of perturbation theory. Many believe that pseudo-Nambu-Goldstone bosons are the simplest way to have ultralow mass, spin-0 particles that are natural in a quantum field theory sense. An additional attraction of the model is that the parameters of the PNGB model might be related to the fundamental Planck and electroweak scales in a way that solves the cosmic coincidence problem [19].

The potential of the PNGB field is well approximated by

$$V = M^4\left[\cos\left(\frac{\phi}{f}\right) + 1\right] \tag{6}$$

(where higher derivative terms and instanton corrections are ignored) and is illustrated in Fig. 2. The evolution of the dark energy is controlled by the two parameters of the PNGB potential, M^4 and f, and the initial conditions, ϕ_I and $\dot{\phi}_I$. We take $\dot{\phi}_I = 0$, since we expect the high expansion rate of the early universe to rapidly damp nonzero values of $\dot{\phi}_I$. The initial value of the field, ϕ_I, takes values between 0 and πf. This is because the potential is periodic and symmetric. Since a starting point of ϕ_I/f on the potential is equivalent to starting at $n\pi - \phi_I/f$ and rolling in the opposite direction down the potential, we require $0 < \phi_I/f < \pi$.

Additionally, we place the bound $f < M_p$. As will be discussed in the following section, this is necessary to cut off a divergent direction so that the MCMC chains converge. There are theoretical reasons for this bound as well. For one, it is valid to neglect higher derivative terms of the PNGB potential, Eq. (6), at least as long as $f < M_p$. In general, we do not expect to understand $4-D$ effective field theory at energies much larger than this. Additionally, there are indications from string theory that f cannot be larger than M_p [20,21].

III. ANALYSIS AND MCMC

Following the DETF methodology, we generate data sets for future supernova, weak gravitational lensing, baryon acoustic oscillation, and cosmic microwave background observations. These observations are forecasted for three experimental stages: Stage 2 represents in-progress projects relevant to dark energy; Stage 3 refers to medium-sized experiments; Stage 4 comprises larger dark energy projects including a large ground-based survey (LST), and/or a space-based program. (Stage I, not considered in our analysis, represents already completed dark energy experiments, and is less constraining than Stage 2 data.) "Optimistic" and "pessimistic" versions of the same simulated data sets give different estimates of the systematic errors. More information on the specific data models is given in Appendix A (or see also the technical appendix of the DETF report [3]). In our work we did not use the cluster data because of the difficulty of adapting the DETF construction to a quintessence cosmology (the same reasons given in [4]).

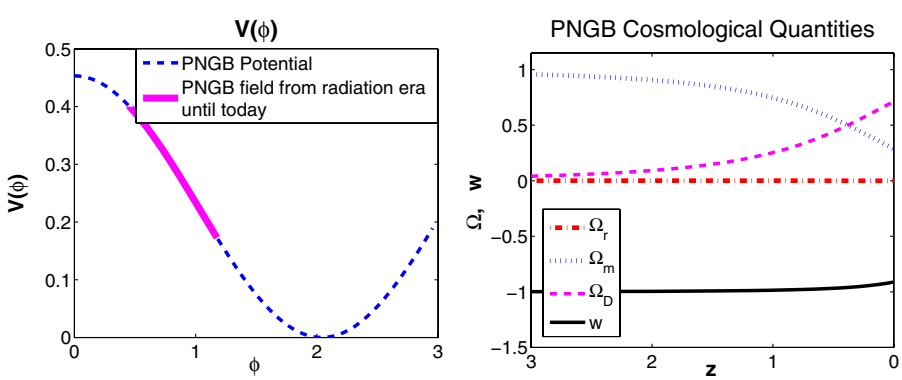

FIG. 2 (color online). An example of a PNGB model and its resulting cosmological solution for typical values of the PNGB parameters. The PNGB potential $V(\phi)$ (dashed curve, right panel) is in units of h^2. The evolution of the PNGB field along the potential since the radiation era is shown by the solid curve overlaying the potential. The energy densities in the right panel are related to these units via $\Omega = \omega/h^2$.

We generate and analyze two versions of data. One is built around a cosmological constant model of the universe. The other is based on a PNGB fiducial model. The latter is chosen to be consistent with a cosmological constant for Stage 2 data.

We use Markov Chain Monte Carlo analysis with a Metropolis-Hastings stepping algorithm [22–24] to evaluate the likelihood function for the parameters of our model. The details of our methods are discussed in Appendix B. MCMC lends itself to our analysis because our probability space is both non-Gaussian and also depends on a large number of parameters. These include the PNGB model parameters: M^4, f, and ϕ_I, the cosmological parameters: ω_m, ω_k, ω_B, δ_ζ, n_s (as defined by the DETF), and the various nuisance and/or photo-z parameters accounting for error and uncertainties in the data).

In order for the results of an MCMC chain to be meaningful, there must exist a finite, stationary distribution to which the Markov chain may converge in a finite number of steps. Degeneracies between parameters, i.e., combinations of different parameters that give rise to identical cosmologies, correspond to unconstrained directions in the probability distribution. Unless some transformation of parameters is found and/or a cutoff placed on these parameters, the MCMC will step infinitely in this direction and can never converge to a stationary distribution. Additionally, the shape of the probability distribution can drastically affect the efficiency of the chain. A large portion of the task of analyzing the PNGB model, therefore, involves finding convenient parametrizations and cutoffs to facilitate MCMC exploration of the posterior distribution.

The probability space of the PNGB model becomes more tractable from an MCMC standpoint if we transform from the original variables to ones that are more directly related to cosmological observables constrained by the data. Such parametrizations make it easier to identify degeneracies and also tend to make the shape of the probability distribution more Gaussian. As discussed in Sec. II, the dynamics of the PNGB field depend on its potential $V(\phi) = M^4(\cos(\frac{\phi}{f}) + 1)$, and the specific values of M^4, f, and ϕ_I. In order to fit current data the field must hang on the potential approximating a cosmological constant for most of the expansion history of the universe. If the field never rolls it acts as a cosmological constant for all times with a value corresponding to the initial energy density of the field, $V_I = V(\phi_I)$. To first order, then, V_I sets the overall scale of the dark energy density. Since V_I has more physical significance than M^4, it is a more efficient choice for our MCMC analysis.

Additionally, the "phase" ϕ_I/f of the field's starting point in the cosine potential is closely related to the initial slope of the potential. The slope affects the time scale on which the field will evolve. If, for instance, $\phi_I/f = 0$ the

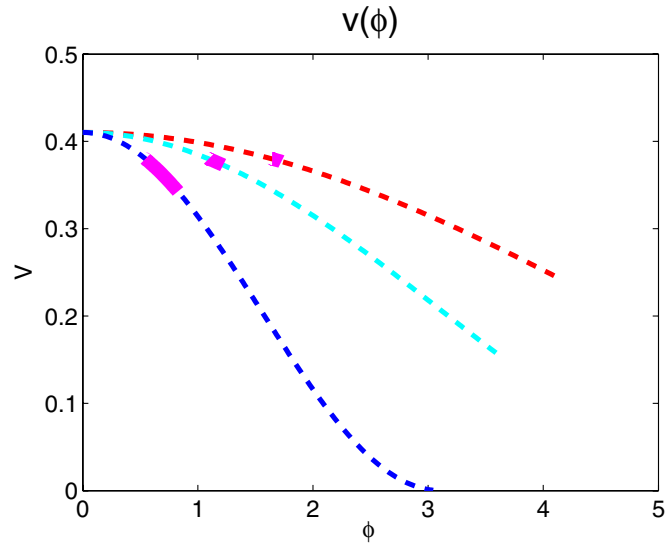

FIG. 4 (color online). PNGB potentials (dashed line) and with the entire field evolution shown in thick solid curves. The different curves show increasing values of f from left to right. The smallest value of f (bottom curve) gives a nearly static dark energy and fits a cosmological constant well. Any larger value for f will also fit the data because the potential will be flatter, and the field will evolve even less.

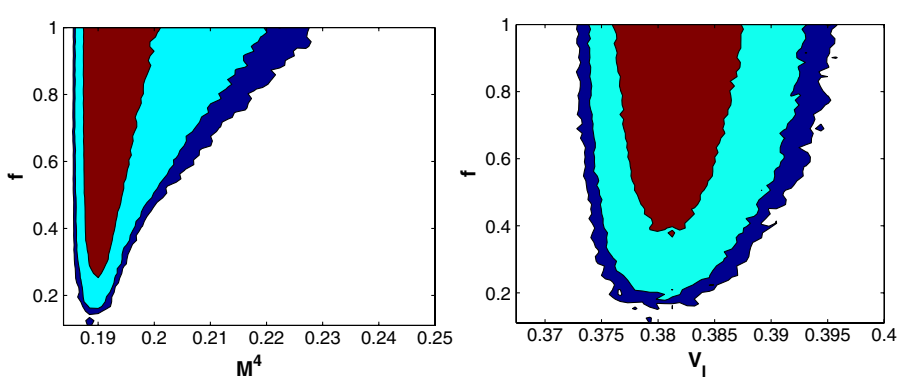

FIG. 3 (color online). $2-D$ confidence regions for f vs M^4 (left panel) and f vs V_I (right panel). The concave feature of the f vs M^4 contours means it is inefficiently explored by MCMC. Contours in the $f - V_I$ space are nearly Gaussian and better facilitate convergence.

field starts out on the very top of the potential where the slope is exactly zero, and the field will not evolve. Starting closer to the inflection point of the potential results in a steeper initial slope and the field will roll faster toward the minimum. Since the variable ϕ_I can correspond to both flat initial slopes (if f is large) or steep ones (if f is small), ϕ_I/f is more directly related to the dynamics of the field and is therefore a superior parameter choice. These new parameters, as illustrated in Fig. 3, also result in a probability distribution that is more Gaussian and thus is more easily explored by our MCMC algorithm.

Even more important than choosing physically relevant parameters is deciding how to handle divergent directions in probability space. For PNGB quintessence the parameter f must be cut off in some way because it can become arbitrarily large without being constrained by the data. For the fiducial model based on a ΛCDM universe, solutions where the field does not evolve for the entire expansion history of the universe, i.e., behaves as a cosmological constant, can fit the forecast data perfectly. If such a choice of parameters is found, then larger and larger values of f will only make the potential flatter and flatter. If the field did not evolve significantly for the smaller values of f, this will be even more true as the potential flattens. Hence, f can become arbitrarily large and the cosmological observables will remain identical, as shown in Fig. 4.

In general, it is possible to achieve identical deviations from a cosmological constant by increasing f while at the same time moving ϕ_I/f towards the inflection point of the potential. Increasing f flattens the potential, but by changing ϕ_I/f, the slope of the potential can be held nearly constant and the evolution of the field will not change significantly. In order to achieve results with MCMC, it is necessary to choose some cutoff f so that this infinite direction is bounded. We choose $f < M_p$ because there is some theoretical motivation for this choice as detailed in Sec. II.

IV. RESULTS

A. ΛCDM Fiducial model

In this section we present the results of our MCMC analysis for the combined data sets based on a ΛCDM fiducial model. The model parameters (represented in Table I) are in units of h^2.

Stage 2 combines supernovae, weak lensing, and cosmic microwave background (CMB) data. Stages 3 and 4 additionally include baryon acoustic oscillation (BAO) data. We marginalize over all but two parameters to calculate $2-D$ contours for parameters of the PNGB model and find the 68.27%, 95.44%, and 99.73% (1, 2, and 3 sigma) confidence regions.

Figure 5 depicts the contours in the V_I-ϕ_I/f plane for Stage 2, and the optimistic versions of Stage 3, Stage 4 space, and Stage 4 LST-ground combined data. The horizontal axis where $\phi_I/f = 0$ corresponds to a cosmological constant. (As explained above, the field is starting exactly at the top of its potential and does not roll because the potential is flat at this point.)

TABLE I. ΛCDM fiducial parameter values (left column) and PNGB fiducial parameter values (right column). The nuisance and photo-z parameters are 0 for each. $\omega_{\rm DE}$ is the same as V_I for a ΛCDM universe and $\omega_{\rm DE} = 0.3738$ for the PNGB fiducial universe displayed in the right column. The value of f in the left column is left blank since it is inconsequential for a ΛCDM universe. Energy densities and V_I are in units of h^2. f is in reduced Planck units.

ω_m	0.146	0.145
ω_k	0.0	0.0
ω_B	0.024	0.024
n_s	1.0	1.0
δ_ξ	0.87	0.87
V_I	0.1898	0.4319
$\frac{\phi_I}{f}$	0	0.8726
f	—	0.7103

The value of V_I on this axis, therefore, represents the dark energy density, $\omega_{\rm DE}$, or Λ. The contours, as expected, are centered around $V_I = .38$, the fiducial value of $\omega_{\rm DE}$. It can be seen that the area of the contours shrinks from Stage 2 to Stage 3 and again from Stage 3 to Stage 4. The shrinking in the ϕ_I/f direction roughly corresponds to constraining deviations from a cosmological constant. (Although this interpretation is a slight oversimplification, since for larger values of f, ϕ_I/f can be nonzero and perceptible deviations from a cosmological constant will not occur until sometime in the future.) The reduction in the V_I direction reflects constraints the data places on the contribution from the dark energy to the energy density of the universe.

Figure 6 depicts the $f - \phi_I/f$ contours. Although all values of f are allowed, as f approaches zero the PNGB potential gets narrower, and the phase must start closer to zero, or else the field will evolve too quickly to its vacuum state. (The very thin part of the distribution close to $f = 0$ is not resolved by the MCMC analysis.) For larger values of f, ϕ_I/f may start further from the peak of the potential without the field evolving much. Even for Stage 2, however, the field may not start past the inflection point of the potential.

Often it is assumed that the PNGB field is initially displaced a small amount from the potential minimum. But with the constraint we have placed on f, this region of parameter space is no longer accessible for data based on a ΛCDM fiducial model. This is because as the field starts lower down the slope of the potential, the peak of the potential must be raised so that V_I may reflect the approximate energy density needed by the dark energy. But as the peak of the potential gets higher it also becomes steeper (since f is bounded) and the field evolves too quickly to fit the data. It has been suggested, however, that since we

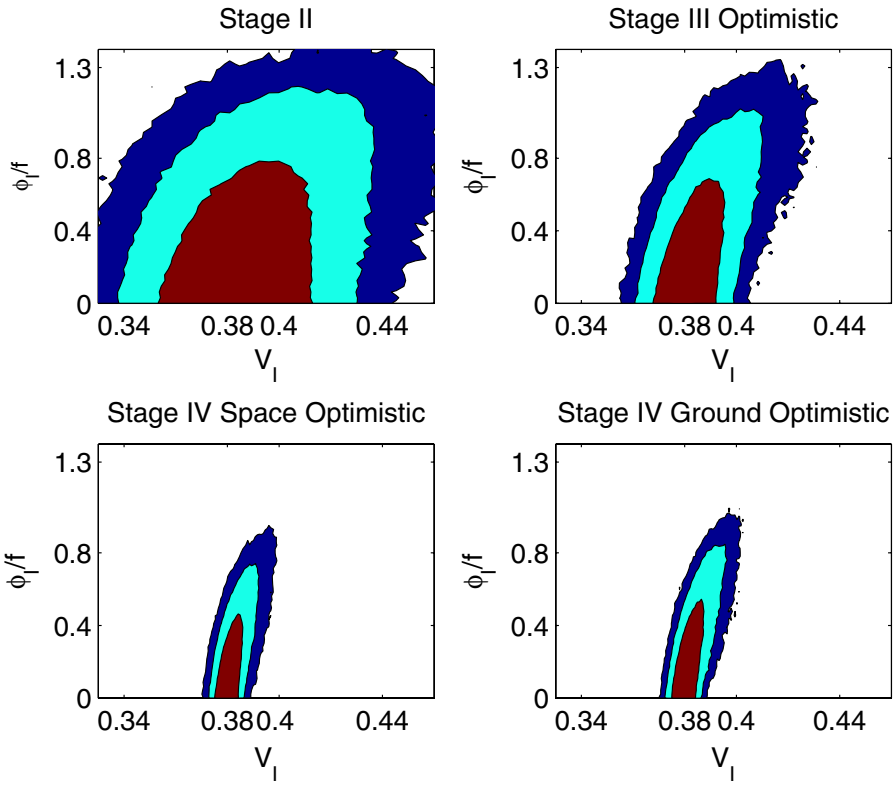

FIG. 5 (color online). $V_I - \phi_I/f$ 1, 2, and 3 sigma confidence regions for DETF optimistic combined data sets.

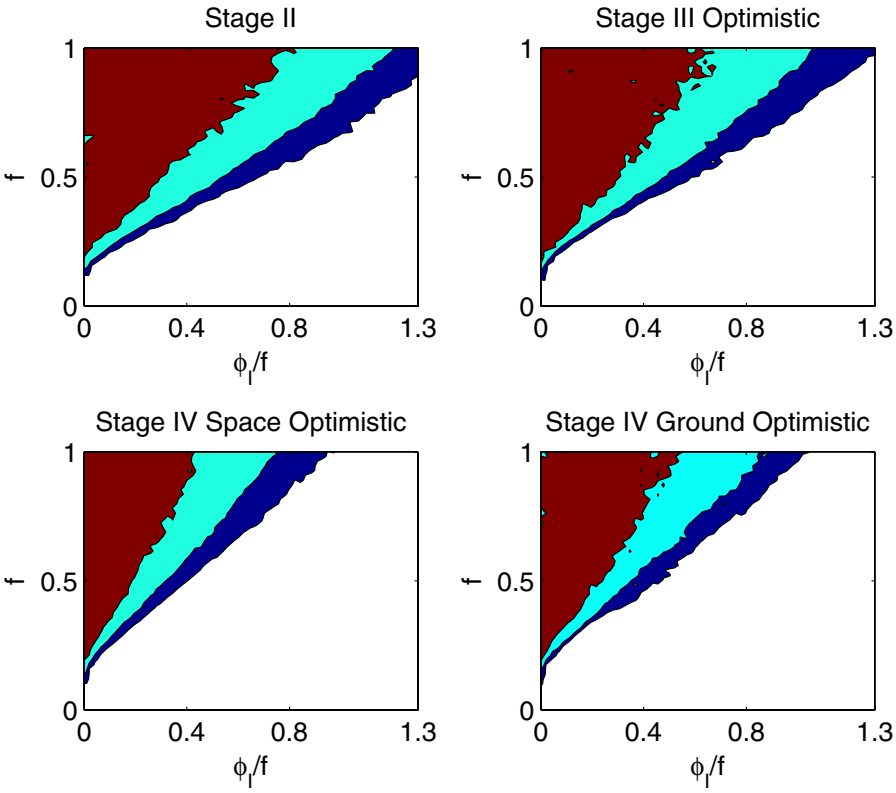

FIG. 6 (color online). $f - \phi_I/f$ 1, 2, and 3 sigma confidence regions for DETF optimistic combined data sets.

expect quantum fluctuations to displace the field from the top of potential, it is more reasonable to expect the PNGB field to start after the inflection point of the potential [16]. If either this argument or the theoretical reasons for the bound $f < M_p$ could be made more convincing, experimental results consistent with a cosmological constant could potentially rule out the PNGB model. As it stands, however, we do not feel the arguments constraining f and ϕ_I are robust enough to make such a claim.

Figure 7 depicts V_I versus $\delta\omega_{\rm DE}$, where $\delta\omega_{\rm DE} = V_I - \omega_{\rm DE}(a = 1)$. Since PNGB quintessence is a "thawing" model of dark energy [25], that is, it starts as a cosmological constant until the field begins to roll causing the amount of dark energy to decrease, $\delta\omega_{\rm DE}$ reflects the amount the dark energy has deviated from a cosmological constant. As the DETF found, subsequent stages of data do better at constraining the evolution of the dark energy. The fact that Stage 4 space seems a little more constraining than ground reflects the fact that ground and space data are sensitive to slightly different features in the dark energy evolution and will be more or less powerful at different redshifts. Other quintessence models, such as the Albrecht-Skordis model

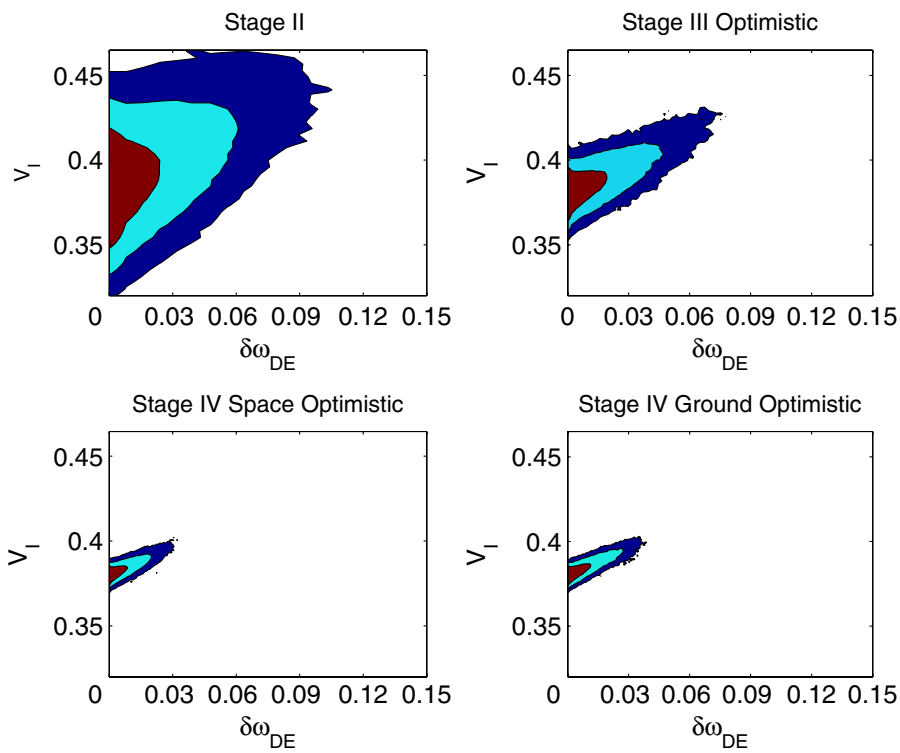

FIG. 7 (color online). $V_I - \delta\omega_{\rm DE}$ 1, 2, and 3 sigma confidence regions for optimistic combined data. Here $\delta\omega_{\rm DE}$ is the amount of change in the dark energy density from the radiation era until today.

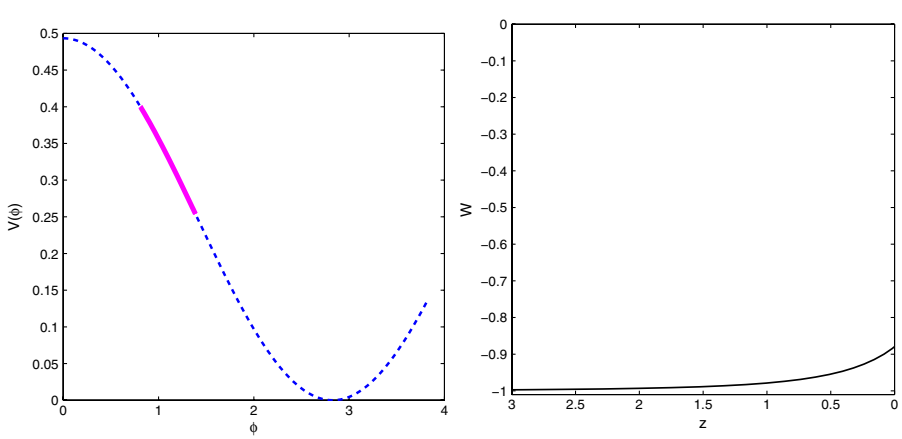

FIG. 8 (color online). The evolution of the PNGB fiducial model field (left panel, solid curve) in the PNGB potential (dashed curve). The corresponding equation of state evolution is shown in the right panel.

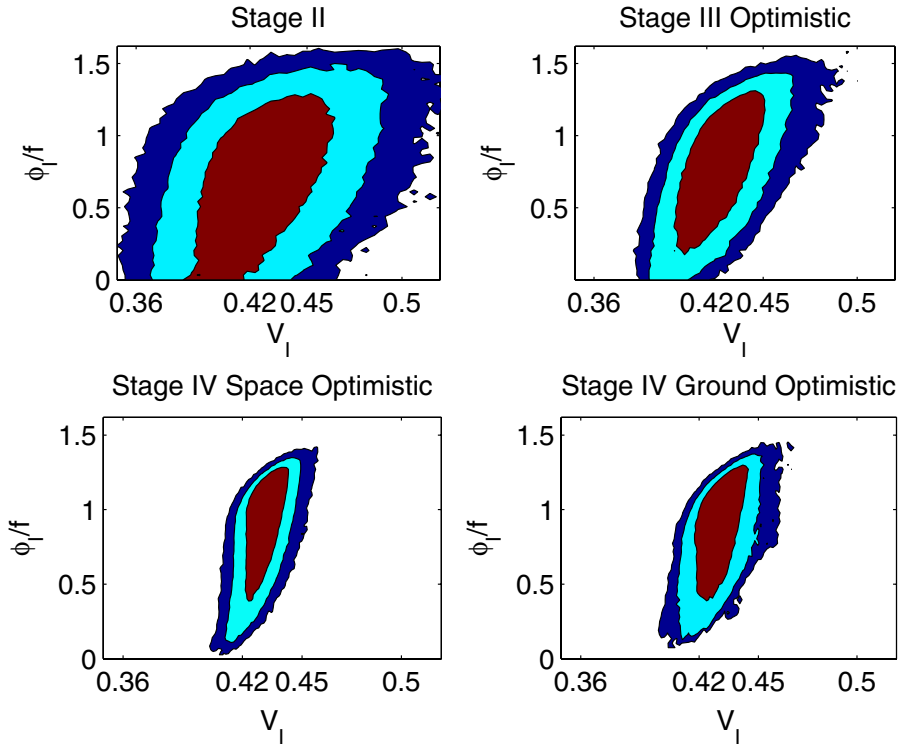

FIG. 9 (color online). $V_I - \phi_I$ 1, 2, and 3 sigma confidence regions for DETF optimistic combined data sets using the PNGB background cosmological model.

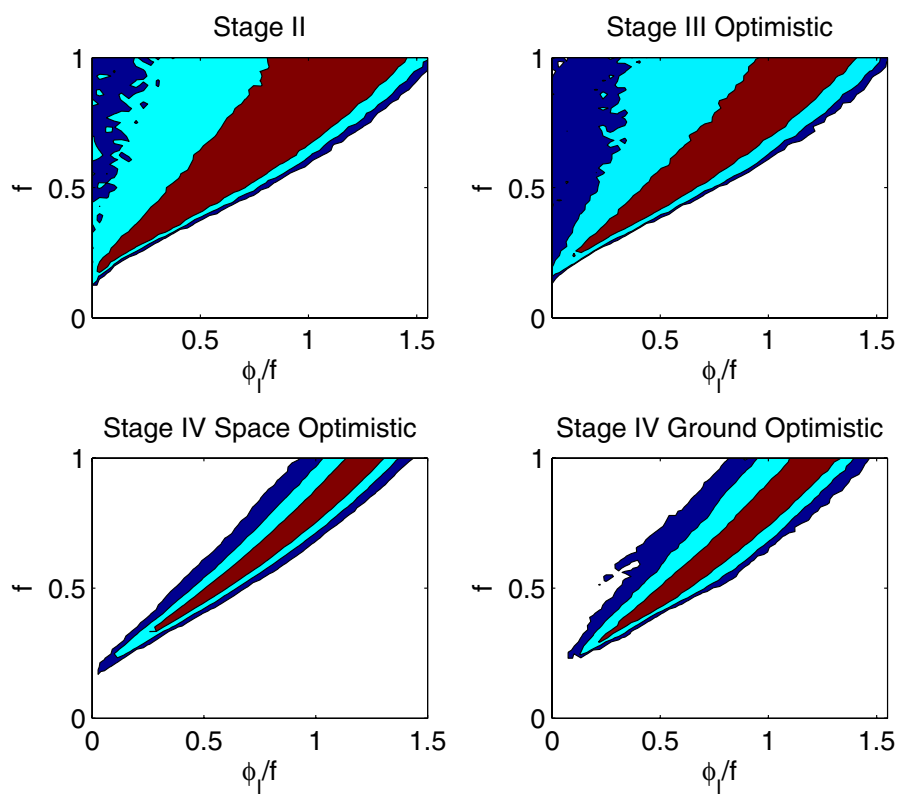

FIG. 10 (color online). $f - \phi_I/f$ 1, 2, and 3 sigma confidence regions for DETF optimistic combined data sets using the PNGB background cosmological model.

[9] are somewhat better constrained by the DETF Stage 4 ground data models than by DETF Stage 4 space.

B. PNGB fiducial model

In addition to considering a ΛCDM fiducial model, we evaluate the power of future experiments assuming the dark energy is really due to PNGB quintessence. Our PNGB fiducial parameter values (shown in Table I in units of h^2) were chosen such that the fiducial model lies within the 95% confidence region for Stage 2 ΛCDM data, but demonstrates a small amount of dark energy evolution that can be resolved by Stage 4 experiments.

The left panel of Fig. 8 shows the potential and evolution of the field for this model. The right panel depicts $w(z)$. It can be seen that today ($z = 0$) the deviation of the field from $w(z) = -1$ is only about 10%.

Repeating our MCMC analysis for the PNGB fiducial model, we again marginalize over all but two parameters to depict the 2-d confidence regions for the dark energy parameters. Figure 9 depicts the $V_I - \phi_I/f$ contours. It can be seen that the $\phi_I/f = 0$ axis corresponding to the field sitting on the top of its potential and not evolving, is allowed at Stage 2 but becomes less favored by subsequent stages of the data. By Stage 4 it is ruled out by more than 3σ.

Figure 10 depicts the $\phi_I/f - f$ contours. Again it can be seen that for larger values of f, ϕ_I/f must be nonzero. By Stage 4 optimistic, only extreme fine-tuning with f allows ϕ_I/f to approach zero, so that the field will be displaced from the top of the potential and have started to roll by just the right amount by late times.

Figure 11 depicts V_I versus $\delta\omega_{\rm DE}$. At Stage 2 $\delta\omega_{\rm DE} = 0$ is still is within the 1σ confidence region. But subsequent stages of the data disfavor this result. Stage 4 optimistic rules out zero evolution of the dark energy by more than 3σ.

V. DISCUSSION AND CONCLUSIONS

With experiments such as the ones considered by the DETF on the horizon, data sets will be precise enough to make it both feasible and important to analyze dynamic models of dark energy. The analysis of such models, therefore, should play a role in the planning of these experiments.

With our analysis of PNGB quintessence, we have shown how future data can constrain the parameter space of this model. We have shown likelihood contours for a selection of combined DETF data models, and found the increase in parameter constraints with increasing data quality to be broadly consistent with the DETF results in $w_0 - w_a$ space. Direct comparison with the DETF figures of merit is nontrivial because PNGB quintessence depends on three parameters, whereas the DETF FoM were calculated on the bases of two, but in our two dimensional projections we saw changes in the area that are consistent with DETF results. Specifically, the DETF demonstrated a

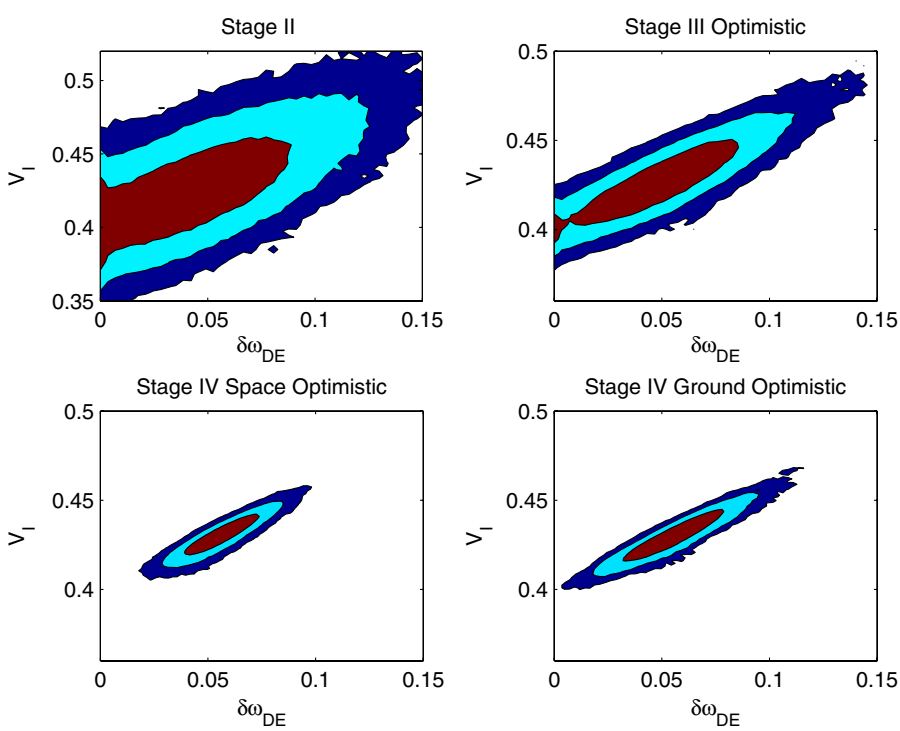

FIG. 11 (color online). $V_I - \delta\omega_{\rm DE}$ 1, 2, and 3 sigma confidence regions for DETF optimistic combined data, where $\delta\omega_{\rm DE}$ is the amount of change in the dark energy density from the radiation era until today.

factor of roughly three decrease in allowed parameter area when moving from Stage 2 to good combinations of Stage 3 data, and a factor of about ten in area reduction when going from Stage 2 to Stage 4. We saw decreases by similar factors in our two dimensional projections. We have presented likelihood contour plots for specific projected data sets as an illustration. In the course of this work we produced many more such contour plots to explore the other possible data combinations considered by the DETF including the data with pessimistic estimates of systematic errors. We found no significant conflict between our results in the PNGB parameter space and those of the DETF in $w_0 - w_a$ space.

As discussed in [15], we believe the fact that we have demonstrated (here and elsewhere [8,9]) results that are broadly similar to those of the DETF despite the very different families of functions $w(a)$ considered is related to the fact pointed out in [4] that overall the good DETF data sets will be able to constrain many more features of $w(a)$ than are present in the $w_0 - w_a$ ansatz alone.

As data continues to improve, MCMC analysis of dynamic dark energy models will likely become more popular. Our experience with the PNGB model could be relevant to future work. We find that the theoretical parameters of the model are not in general the best choice for MCMC. Transforming to variables that are closely related to the physical observables can help MCMC converge more efficiently. Additionally, it is necessary to cut off unconstrained directions in parameter space. It would be desirable to find bounds that have some physical motivation. For PNGB quintessence, we find that the initial value of the potential, $V(\phi_I)$, and the initial phase of the field, ϕ_I/f, are more convenient than the original model parameters, and that there is some motivation for placing the bound $f < M_p$.

Finally, we have demonstrated the power Stage 4 data will have for detecting time evolution of the dark energy. The PNGB fiducial model we choose is consistent with Stage 2 data (and with current data by extension). If, however, the universe were to in fact be described by such a dark energy model, then by Stage 4 we would know to better than 3 sigma that there is a dynamic component to the dark energy.

ACKNOWLEDGMENTS

We thank Matt Auger, Lloyd Knox, and Michael Schneider for useful discussions and constructive criticism. Thanks also to Jason Dick who provided much useful advice on MCMC. We thank the Tony Tyson group for use of their computer cluster, and, in particular, Perry Gee and Hu Zhan for expert advice and computing support. Gary Bernstein provided us with Fischer matrices suitable for adapting the DETF weak lensing data models to our methods, and David Ring and Mark Yashar provided additional technical assistance. This work was supported by DOE Grant No. DE-FG03-91ER40674 and NSF Grant No. AST-0632901.

APPENDIX A: DATA

For each step in the MCMC chain, we integrate numerically to calculate the theoretical quantities dependent on the dark energy. We start our integration at early times with $a = 10^{-15}$ and we end the calculation at $a = 2$. We compare these values with the observables generated based on our fiducial models. With the uncertainties in the data forecast by the DETF we can calculate the likelihood for each step in the chain. What follows is an overview of the likelihood calculation for each type of observation we consider.

1. Type 1a supernovae

After light curve corrections, supernovae observations provide the apparent magnitudes, m_i, and the redshift values, z_i, for supernova events. The apparent magnitudes are related to the theoretical model through the distance modulus, $\mu(z_i)$, by

$$m_i = M + \mu(z_i), \tag{A1}$$

where

$$\mu(z_i) = 5\log_{10}(d_l(z_i)) + 25, \tag{A2}$$

M is the absolute magnitude, and

$$d_L(z_i) = \frac{1}{a}\begin{cases} \frac{1}{\sqrt{|k|}}\sinh(\sqrt{|k|}\chi(z_i)) & k < 0 \\ \chi(z_i) & k = 0 \\ \frac{1}{\sqrt{|k|}}\sin(\sqrt{|k|}\chi(z_i)) & k > 0 \end{cases} \tag{A3}$$

and

$$\chi(z_i) = \eta_0 - \eta(z_i) \equiv \int_{a_i}^{1} \frac{da}{a^2 H(a)} \tag{A4}$$

with $|k| = H_0^2|\Omega_k| = (\frac{H_0}{h})^2|\omega_k|$.

Uncertainties in absolute magnitude M as well as the absolute scale of the distance modulus lead to the introduction of an offset $\mu_{\rm off}$ nuisance parameter in all SNe data sets, giving $\mu(z_i) \to \mu(z_i) + \mu_{\rm off}$.

Other systematic errors are modeled by more nuisance parameters. The peak brightness of supernovae, for instance, may have some z-dependent behavior that is not fully understood. We include this uncertainty in our analysis by allowing the addition of small linear and quadratic offsets in z. Additionally, each SNe data model combines a collection of nearby supernovae with a collection of more distant ones. Possible differences between the two groups are modeled by considering the addition of a constant offset to the near group. The distance modulus becomes

$$\mu(z_i)_{\rm calc} = \mu(z_i) + \mu_{\rm off} + \mu_{\rm lin} z_i + \mu_{\rm quad} z_i^2 + \mu_{\rm shift} z_{\rm near}. \tag{A5}$$

In addition, some experiments will measure supernovae redshifts photometrically instead of spectroscopically. There may be a bias in the measurement of the photo-z's in each bin. This uncertainty is expressed by another set of nuisance parameters, δz_i, that can shift the values of each z_i. These observables become $\mu_i = \mu(z_i + \delta z_i)$.

Priors are assigned to each of the nuisance parameters (except for $\mu_{\rm off}$, which is left unconstrained) which reflect the projected strength of the various observational programs. Additionally, statistical errors are presumed to be Gaussian and are given by the diagonal covariance matrix $C_{ij} = \sigma_i^2$, where σ_i reflects the uncertainty in the μ_i observables for each data set.

The likelihood function L for the supernovae data can be calculated from the chi-squared statistic, where $\chi^2 \equiv -2\ln L$. For data sets with photometrically determined redshifts chi-squared is

$$\chi^2 = \sum \frac{(\mu(z_i + \delta z_i) - \mu(z_i)_{\rm data})^2}{\sigma_i^2} + \frac{\mu_{\rm lin}^2}{\sigma_{\rm lin}^2} + \frac{\mu_{\rm quad}^2}{\sigma_{\rm quad}^2} + \frac{\mu_{\rm near}^2}{\sigma_{\rm near}^2} + \sum\left(\frac{\delta z_i^2}{\sigma_{z_i}^2}\right). \tag{A6}$$

For data sets with spectroscopic redshifts the chi-squared is the same minus the contribution from redshift shift parameters.

2. Baryon acoustic oscillations

Large scale variations in the baryon density in the universe have a signature in the matter power spectrum that when calibrated via the CMB provides a standard ruler for probing the expansion history of the universe. The observables for BAO data (after extraction from the mass power spectrum) are the comoving angular diameter distance, $d_a^{\rm co}(z_i)$, and the expansion rate, $H(z_i)$, where

$$d_a^{\rm co} = a d_L \tag{A7}$$

and z_i indicates the z bin for each data point. The quality of the data probe is modeled by the covariance matrix for each observable type, as described in Sec. 4 of the DETF technical appendix. Additionally, some BAO observations use photometrically determined redshifts, in which case δz_i are added as nuisance parameters as for the supernovae, to describe the uncertainty in each redshift bin.

The likelihood function for BAO observations is

$$\chi^2 = \sum \frac{(d_a^{\rm co}(z_i + \delta z_i) - d_{a\text{-}\rm data}^{\rm co}(z_i))^2}{\sigma_{di}^2} + \sum \frac{(H(z_i + \delta z_i) - H_{\rm data}(z_i))^2}{\sigma_{Hi}^2} + \sum \frac{\delta z_i^2}{\sigma_{z_i}^2}. \tag{A8}$$

3. Weak gravitational lensing

Light from background sources is deflected from a straight path to the observer by mass in the foreground. From high resolution imaging of large numbers of galaxies, it is possible to detect statistical correlations in the stretching of galaxies, "cosmic shear." From this foreground mass distributions can be determined. The mass distribution as a function of redshift provides a probe of the growth history of density perturbations, $g(z)$, where $g(z)$ (in linear perturbation theory) depends on dark energy via

$$\ddot{g} + 2H\dot{g} = \frac{3\Omega_m H_o^2}{2a^3} g. \tag{A9}$$

Additionally, because the amount of lensing depends on the ratios of distances between the observer, the lens and the source, gravitational lensing also probes the expansion history of the universe, $D(z)$.

The direct observables of weak lensing surveys considered by the DETF are the power spectrum of the lensing signal and the cross correlation of the lensing signal with foreground structure. Systematic and statistical uncertainties are described by a Fisher matrix in this space. As is detailed in the DETF appendix, it is possible to transform from this parameter space to the variables directly dependent on dark energy, $g(z)$ and $D(z)$. These become the weak lensing observables we use in our analysis.

In addition to depending on the dark energy model, weak lensing observations depend on the cosmological parameters matter density ω_m, baryon density ω_B, effective curvature density ω_k, the spectral index n_S, and the amplitude of the primordial power spectrum δ_ζ. These parameters are treated as nuisance parameters with priors imposed by the Fisher matrix.

Last, since ground-based lensing surveys will photometrically determine redshifts, as for SNe and BAO data, we must model the uncertainty in redshift bins. Again this is done by allowing each z_i bin to vary by some amount δz_i.

The weak lensing observables are given to be the vector

$$\vec{X}_{\rm obs} = [(\omega_m, \omega_k, \omega_B, n_s, \delta_\zeta), d_a^{\rm co}(z_i), g(z_i), \ln(a(z_i))], \tag{A10}$$

where $a(z_i)$ is the scale factor corresponding to the redshift bins for the data. The error matrix is nondiagonal in the space of these observables so chi-squared is given by

$$\chi^2 = (\vec{X}_{\rm obs} - \vec{X}_{\rm obs\text{-}data})\mathbf{F}_{\rm \mathbf{lensing}}(\vec{X}_{\rm obs} - \vec{X}_{\rm obs\text{-}data})^{\top}. \tag{A11}$$

4. Planck CMB

As with baryon oscillations, observations of anisotropies in the cosmic microwave background probe the expansion history of the universe by providing a characteristic length scale at the time of last scattering. As with weak lensing, our Planck observables are extrapolated from the CMB

temperature and polarization maps. The observable space constrained by Planck becomes: n_s, ω_m, ω_B, δ_ζ, $\ln(\Theta_S)$. These variables are constrained via the Fisher matrix in this space (we use the same one used in [4]). The chi-squared is calculated as

$$\chi^2 = (\vec{X}_{\rm obs} - \vec{X}_{\rm obs\text{-}data})\mathbf{F}_{\mathbf{Planck}}(\vec{X}_{\rm obs} - \vec{X}_{\rm obs\text{-}data})^{\top}. \tag{A12}$$

APPENDIX B: MCMC

Markov Chain Monte Carlo simulates the likelihood surface for a set of parameters by sampling from the posterior distribution via a series of random draws. The chain steps semistochastically in parameter space via the Metropolis-Hastings algorithm such that more probable values of the space are stepped to more often. When the chain has converged it is considered a "fair sample" of the posterior distribution, and the density of points represents the true likelihood surface. (Explanations of this technique can be found in [22,26,27]).

With the Metropolis-Hastings algorithm, the chain starts at an arbitrary position θ in parameter space. A candidate position θ' for the next step in the chain is drawn from a proposal probability density $q(\theta, \theta')$. The candidate point in parameter space is accepted and becomes the next step in the chain with the probability

$$\alpha(\theta, \theta') = \min\left\{1, \frac{P(\theta')q(\theta', \theta)}{P(\theta)q(\theta, \theta')}\right\}, \tag{B1}$$

where $P(\theta)$ is the likelihood of the parameters given the data. If the proposal step θ' is rejected, the point θ becomes the next step in the chain. Although many distributions are viable for the proposal density $q(\theta, \theta')$, for simplicity we have chosen to use a Gaussian normal distribution. (It should be noted that, in general, the dark energy parameters of the model are not Gaussian distributed. The power of the MCMC procedure lies in the fact that it can probe posterior distributions that are quite different from the proposal density $q(\theta, \theta')$.) Since this is symmetric, $q(\theta, \theta') = q(\theta', \theta)$, we need only consider the ratios of the posteriors in the above stepping criterion.

For the results of the Markov chain to be valid, it must equilibrate, i.e., converge to the stationary distribution. If such a distribution exists, the Metropolis-Hastings algorithm guarantees that the chain will converge as the chain length goes to infinity. In practice, however, we must work with chains of finite length. Moreover, from the standpoint of computational efficiency, the shorter our chains can be and still reflect the true posterior distribution of the parameters, the better. Hence a key concern is assuring that our chains have equilibrated. Though there are many convergence diagnostics, chains may only fail such tests in the case of nonequilibrium; none guarantee that the chain has converged [28]. We therefore monitor the chains in a variety of ways to convince ourselves that they actually reflect the underlying probability space.

Our first check involves updating our proposal distribution $q(\theta, \theta')$, which we have already chosen to be Gaussian normal. Each proposal step is drawn randomly from this distribution. The size of the changes generated in any given parameter direction depend on the covariance matrix we use to define $q(\theta, \theta')$. We start by guessing the form of the covariance matrix and run a short chain ($O(10^5)$ steps) after which we calculate the covariance matrix of the Markov chain. We then use this covariance matrix to define the Gaussian proposal distribution for the next chain. We repeat this process until the covariance matrix stops changing systematically. This implies that the Gaussian approximation to the posterior has been found. In addition to indicating convergence, this also assists the efficiency of our chains. The more the proposal distribution reflects the posterior, the quicker the Markov chain will approximate the underlying distribution.

One convergence concern is that we might not be exploring the entire probability space. Since too large of a proposal step can cause excessive rejection of parameter space, we shrink our covariance matrix by a fixed amount to ensure that the small scale features of the posterior are thoroughly probed. However, it then is possible, for instance, that if we started our chains at a random point in probability space and our step sizes are too small, the chain may have wandered to a local maximum from which it will not exit in a finite time. We could be missing other features of the underlying probability space. We convince ourselves that this is not the case by starting chains at different points in parameter space. We find that the chains consistently reflect the same probability distribution, and, hence, we conclude that we are truly sampling from the full posterior.

After we have determined our chains are fully exploring probability space and we have optimized our Gaussian proposal distribution, we run a longer chain to better represent the probability space of our variables. We consider the chain to be long enough when the 95% contour is reasonably smooth. For most data sets, chains of $O(10^6)$ are sufficient although the larger the probability space, the longer the chains must be. (In particular, Stage 4 ground data involves a large number of nuisance parameters and may take two to 3 times longer to return smooth contours.) With the final chains, we must control for both burn-in and correlations between parameter steps. Burn-in refers to the number of steps a chain must take before it starts sampling from the stationary distribution. Because we have already run a number of preliminary chains, we know approximately the mean parameters of our model. We find that the means refer to a point in probability space close to the maximum of the distribution. (Generically, this does not have to be true if the probability space is asymmetrical.) If we use this as our starting point, our chains do not have to wander long before they appear to sample from the sta-

tionary distribution. We control for this by removing different amounts from the start of the chain. For instance, if we cut out the first 1000 steps and calculate the contours and compare this to contours calculated with the first 100 000 steps removed we find that the shape of the $2-D$ contours remain essentially the same. We can conclude, therefore, that chains very quickly begin sampling the posterior distribution and we need not worry about burn-in.

Correlations between steps may also affect the representativeness of the samples generated via MCMC. The effects, however, may be controlled for by either thinning the chains by a given amount or by running chains of sufficient length such that the correlations become unimportant. We experiment with different thin factors (taking every step, every 10th step, and every 50th step and we find very little difference in our results. Hence we conclude that the sampling of our chains are not greatly affected by correlations.

Last, we apply a numerical diagnostic similar to that used by Dick *et al.* [29] to test the conversion of our chains. (This technique is a modification of the Geweke diagnostic [30].) We compare the means calculated from the first 10% of the chain (after burn-in of 1000) to the means calculated from the last 10%. If the chain has converged to the stationary distribution, then these values should be approximately equal. If $\frac{\mathrm{mean}_1(\theta_i)-\mathrm{mean}_2(\theta_i)}{\sigma_{ii}}$ is large, where σ_{ii} is the standard deviation determined by the chain for the parameter θ_i, then the chain is likely to still be drifting. We find that for our chains $\frac{\mathrm{mean}_1(\theta_i)-\mathrm{mean}_2(\theta_i)}{\sigma_{ii}} < .1$ for 95% of the parameters. The remaining parameters are no less than $\frac{\sigma_{ii}}{5}$ away from each other. Coupling this with the qualitative monitoring of the chains described above, we are confident that our chains do a good job of reflecting the posterior probability distribution of our model.

[1] D. Huterer and M. S. Turner, Phys. Rev. D **60**, 081301(R) (1999).
[2] D. Huterer and M. S. Turner, Phys. Rev. D **64**, 123527 (2001).
[3] A. Albrecht *et al.*, arXiv:astro-ph/0609591.
[4] A. Albrecht and G. Bernstein, Phys. Rev. D **75**, 103003 (2007).
[5] D. Huterer and H. V. Peiris, Phys. Rev. D **75**, 083503 (2007).
[6] M. Schneider, L. Knox, H. Zhan, and A. Connolly, Astrophys. J. **651**, 14 (2006).
[7] J. A. Frieman, C. T. Hill, A. Stebbins, and I. Waga, Phys. Rev. Lett. **75**, 2077 (1995).
[8] B. Bozek, A. Abrahamse, A. Albrecht, and M. Barnard, following Article, Phys. Rev. D **77**, 103504 (2008).
[9] M. Barnard, A. Abrahamse, A. Albrecht, B. Bozek, and M. Yashar, preceding Article, Phys. Rev. D **77**, 103502 (2008).
[10] S. M. Carroll, arXiv:astro-ph/0107571.
[11] E. J. Copeland, M. Sami, and S. Tsujikawa, Int. J. Mod. Phys. D **15**, 1753 (2006).
[12] V. Sahni, Classical Quantum Gravity **19**, 3435 (2002).
[13] R. Bousso, Gen. Relativ. Gravit. **40**, 607 (2008).
[14] P. J. Steinhardt, Phys. Scr. **T117**, 34 (2005).
[15] A. Albrecht, AIP Conf. Proc. **957**, 3 (2007).
[16] N. Kaloper and L. Sorbo, J. Cosmol. Astropart. Phys. 04 (2006) 007.
[17] C. F. Kolda and D. H. Lyth, Phys. Lett. B **458**, 197 (1999).
[18] S. M. Carroll, Phys. Rev. Lett. **81**, 3067 (1998).
[19] L. J. Hall, Y. Nomura, and S. J. Oliver, Phys. Rev. Lett. **95**, 141302 (2005).
[20] M. Dine, arXiv:hep-th/0107259.
[21] T. Banks, M. Dine, P. J. Fox, and E. Gorbatov, J. Cosmol. Astropart. Phys. 06 (2003) 001.
[22] D. Gamerman, *Markov Chain Monte Carlo: Stochastic Simulation for Bayesian Inference* (Chapman & Hall, London, 1997).
[23] N. Metropolis, A. W. Rosenbluth, M. N. Rosenbluth, A. H. Teller, and E. Teller, J. Chem. Phys. **21**, 1087 (1953).
[24] W. K. Hastings, Biometrika **57**, 97 (1970).
[25] R. R. Caldwell and E. V. Linder, Phys. Rev. Lett. **95**, 141301 (2005).
[26] A. Lewis and S. Bridle, Phys. Rev. D **66**, 103511 (2002).
[27] N. Christensen, R. Meyer, L. Knox, and B. Luey, Classical Quantum Gravity **18**, 2677 (2001).
[28] B. Carlin and M. K. Cowles, J. Am. Stat. Assoc. **91**, 883 (1996).
[29] J. Dick, L. Knox, and M. Chu, J. Cosmol. Astropart. Phys. 07 (2006) 001.
[30] E. Geweke, Evaluating the accuracy of sampling based approaches to the calculation of posterior moments (1992).